AIAA 82-4023

Frequency-Domain Analysis of Flexible Spacecraft Dynamics

S.C. Garg*
Ford Aerospace and Communications Corporation, Palo Alto, Calif.

Dynamics of a generic rigid spacecraft with arbitrary elastic appendages is analyzed in the frequency domain. The usual modal expansions are avoided. An example is developed in detail: pitch/twist dynamics of Hermes. Exact frequency-domain results, when compared with truncated modal expansions, show that better simulation accuracy is possible if modes of the full spacecraft are used, rather than appendage modes. A key benefit of this approach is the ease with which a configuration containing discrete dampers is analyzed.

I. Introduction

THE purpose of this paper is to illustrate some advantages of taking a frequency-domain approach to the analysis of flexible spacecraft dynamics. Virtually all analyses combining dynamics and control are carried out in the time domain. The time domain is indispensable for simulation purposes. However, savings in detail and often greater generality are possible in the frequency domain. The two approaches are complementary, not competing. Frequency-domain concepts have rarely been used, e.g., Poelaert.[1] Like the cited work, we shall consider a generic class of flexible spacecraft for concreteness. In the control systems field also, much recent activity has focused on frequency-domain methods; an excellent discussion is given by MacFarlane.[2]

II. A Generic Problem

The class of spacecraft configurations of interest is illustrated in Fig. 1. Attitude and translational control of the central rigid body is desired. Linearized motion equations for the nonspinning central rigid body are given below. [Note: In this section most symbols are vectors in E^3, $F(r,r_1)$ is a 3×3 matrix; only [s, t, σ, m_a, m_b are scalars.]

$$m_b\ddot{d}=F_e-\Sigma\phi^i \qquad I_b\ddot{\theta}=T_e-\Sigma\tau^i \tag{1}$$

where d is translation of 0 relative to F_i, and θ is a vector of infinitesimal Euler rotations taking F_i to F_b. External force F_e and torque T_e act on the rigid component, and ϕ^i, τ^i are respectively the force and torque exerted (about the rigid-body mass center) on the body by the ith elastic appendage. The appendage geometry is shown in Fig. 2.

The elasticity distribution and vibration characteristics of an appendage are described by either partial differential equations and boundary conditions, or, equivalently, by an integral equation giving deflection $\delta(r)$ due to force f at $r=r_1$ (a superscript i is understood):

$$\delta(r)=\int_A F(r,r_1)f(r_1)\,dr_1 \tag{2}$$

A volume integral is meant. This approach has been presented in Ref. 3. The kernel F is symmetric and positive-definite, since rigid-body modes have been excluded in Eq. (2). It contains information on boundary conditions as well. The deflection δ is taken relative to a frame rigidly fixed at the attachment point.

Let us now assume (although the assumption can be relaxed if necessary) that body and surface forces on the appendages are independent of the small deflection δ. They can then be included in F_e, T_e of Eq. (1). Similarly, active control torques are assumed, relative to which small environmental torques are negligible. The vibration frequencies are usually much greater than the orbit frequency ω_0. If no actuators are located on the appendages, the only forces $f(r_1)$ are then

$$f(r_1)=-\sigma[\ddot{\delta}(r_1,t)+\ddot{d}(t)-(r_1+a)^x\ddot{\theta}] \tag{3}$$

where σ is density, and a denotes the point of attachment of the ith appendage relative to F_b. The symbol $(\ )^x$ is the skew-symmetric matrix isomorphic to the vector $(\ )$.

The conventional approach to solving this problem introduces modal expansions, using either appendage or spacecraft modes, and uses orthogonality to obtain uncoupled equations for the modal coordinates. These are then used to obtain, if

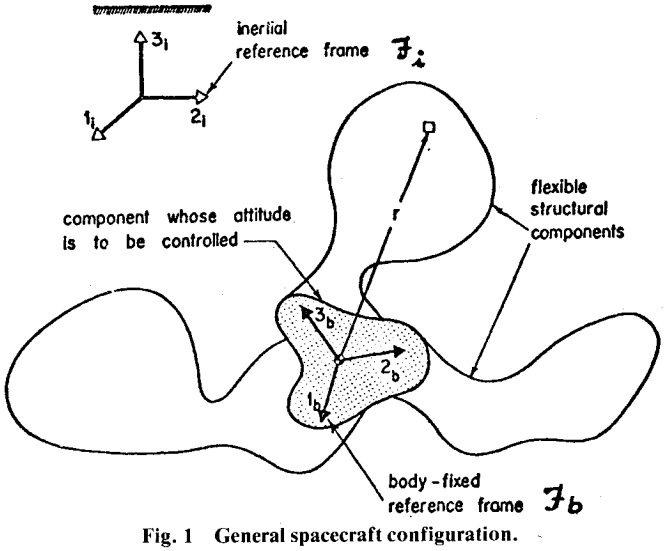

Fig. 1 General spacecraft configuration.

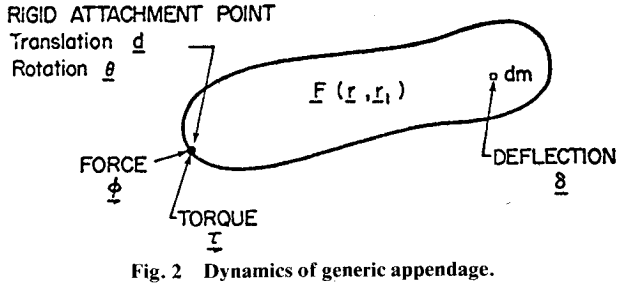

Fig. 2 Dynamics of generic appendage.

Received Aug. 9, 1979; revision received July 28, 1981.

*Principal Engineer, Programs Engineering Dept. Member AIAA.

desired, transfer matrices that contain infinite sums. A general treatment along these lines is given in Ref. 3.

An alternative is to apply the Laplace transform directly to Eqs. (1-3). Substituting Eq. (3) into Eq. (2), and denoting Laplace transforms by a tilde yields

$$\tilde{\delta}(r) + s^2 \int_A F(r,r_1)\tilde{\delta}(r_1)\,\mathrm{d}m = s^2 \int_A F(r,r_1) r_1{}^x \mathrm{d}m\,\tilde{\theta} - s^2 \int_A F(r,r_1)\,\mathrm{d}m\,(d - a^x\tilde{\theta}) \quad (4)$$

Here $\mathrm{d}m = \sigma(r)\,\mathrm{d}r_1$ is a mass element. The solution of this linear equation is obtained by superposition, giving

$$\tilde{\delta}(r) = \tilde{Y}_1(r)\tilde{d} + [\tilde{Y}_2(r) - \tilde{Y}_1(r)a^x]\tilde{\theta} \quad (5)$$

where $\tilde{Y}_1$ and $\tilde{Y}_2$ are transforms which satisfy

$$\tilde{Y}_1(r) + s^2 \int_A F(r,r_1)\,\tilde{Y}_1(r_1)\,\mathrm{d}m = -s^2 \int_A F(r,r_1)\,\mathrm{d}m$$
$$\tilde{Y}_2(r) + s^2 \int_A F(r,r_1)\,\tilde{Y}_2(r_1)\,\mathrm{d}m = s^2 \int_A F(r,r_1) r_1{}^x \mathrm{d}m \quad (6)$$

These integral equations have bounded solutions, except for a discrete set of values of s, if $F(r,r_1)$ is positive definite. $\tilde{Y}_1(r,s)$ and $\tilde{Y}_2(r,s)$ can also be obtained from a differential-equation representation of the appendages. The solutions depend only upon the properties of the ith appendage.

The reaction force ϕ^i and torque τ^i are obtained by balances taken at the attachment point. This requires substitution of Eqs. (5) and (6) into Laplace transformed Eq. (3), and computing net force and torque at the attachment point. In transform notation, one gets

$$\tilde{\phi}(s) = s^2[\tilde{\Phi}_d d(s) + \tilde{\Phi}_\theta \theta(s)] \qquad \tilde{\tau}(s) = s^2[\tilde{T}_d d(s) + \tilde{T}_\theta \theta(s)] \quad (7)$$

where

$$\tilde{\Phi}_d = m_a \mathbf{1} + \int_A \tilde{Y}_1(r)\,\mathrm{d}m \qquad \tilde{\Phi}_\theta = \int_A \tilde{Y}_2(r) - r^x - \tilde{Y}_1(r)a^x \mathrm{d}m$$
$$\tilde{T}_d = \int_A r^x[\tilde{Y}_1(r) + \mathbf{1}]\,\mathrm{d}m \qquad \tilde{T}_\theta = I_a + \int_A r^x[\tilde{Y}_2(r) - a^x]\,\mathrm{d}m \quad (8)$$

Here m_a and I_a respectively the mass and inertia matrix (about the attachment point) of the appendage, and $\mathbf{1}$ is the unit matrix.

It is now possible to write, from Eq. (1), the rigid-body motion equations:

$$(m_b\mathbf{1} + \Sigma\tilde{\Phi}_d^i)\tilde{d} + (\Sigma\tilde{\Phi}_\theta^i)\tilde{\theta} = s^{-2}\tilde{F}_e$$
$$(\Sigma\tilde{T}_d^i)\tilde{d} + (I_b + \Sigma\tilde{T}_\theta^i)\tilde{\theta} = s^{-2}\tilde{T}_e \quad (9)$$

Assembly of these equations is easy once the appendage coefficient matrices are available.

It is emphasized that Eq. (9) holds, regardless of how $\tilde{\Phi}_d^i$, etc., are obtained. Apart from exact solution from an integral or differential-equation approach, expansion in appendage normal modes or approximate methods such as Rayleigh-Ritz, Galerkin, or finite elements may be used. Similarly, the above approach can be readily extended to nonrigid connections, including discrete springs or even dampers. Further extensions can be foreseen to structures involving closed loops, rigid bodies containing rotors, and sensors and actuators mounted on the flexible bodies.

For vehicles having two planes of symmetry, translation and rotation are uncoupled in Eq. (9). Then

$$\tilde{I}_e(s)s^2\theta = \tilde{T}_e \qquad \tilde{I}_e(s) \equiv I_b + \Sigma\tilde{T}_\theta^i(s) \quad (10)$$

and the matrix $I_e(s)$ is termed the "inertance." The results for $\tilde{I}_e(s)$, and also Eq. (9), are directly useful in control-system design and analysis in the frequency domain. In many cases, closed-form results can be obtained from continuum-mechanics analyses of appendages such as flexible solar arrays and antenna booms.

III. A Particular Problem

The utility and economy of the above approach will be illustrated by the pitch/twist dynamics of a satellite with flexible solar arrays of the Hermes type. Modal-expansion results for this problem are discussed in the literature.[4] Figure 3 shows the Hermes satellite and one solar array. The blanket supporting solar cells can be modeled as a membrane in tension. In twisting, the support boom acts as a discrete spring at the array tip. The model of Ref. 4 is generalized here to include dampers at the root and tip. Figure 4 shows the idealized solar array. Following Fig. 2, a reaction torque T is applied at the root, which twists an angle θ. (In this and following sections,

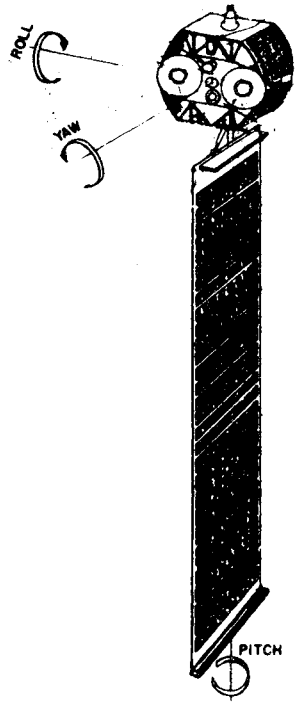

Fig. 3 Hermes spacecraft with one solar array.

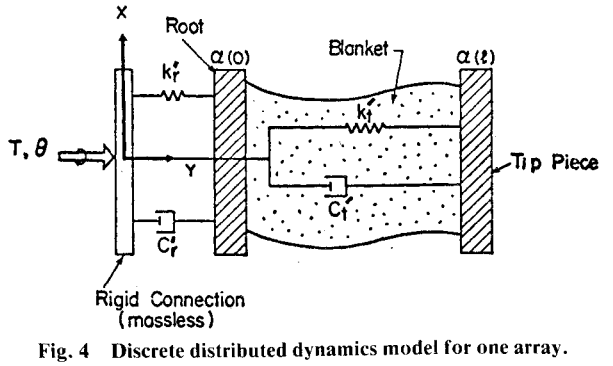

Fig. 4 Discrete distributed dynamics model for one array.

all quantities are scalars—vectors are boldface.) The blanket is under uniform tension P, and has density σ, width w, and deflection $v(x,y) = -x\alpha(y)$. Its motion equation is then

$$P\alpha'' + \sigma w\ddot{\alpha} = \sigma w\ddot{\theta} \tag{11}$$

The motion of the root piece satisfies

$$\frac{1}{12} m_r w^2 [\ddot{\theta} + \ddot{\alpha}(0)]$$

$$= -k_r'\alpha(0) - c_r'\dot{\alpha}(0) + \frac{P}{w}\int_{-w/2}^{w/2} -x^2\alpha'(0)\,dx$$

The last term is the torque due to the membrane. Introducing $k_r = 12k_r'/w^2$, $c_r = 12c_r'/w^2$ and simplifying, this yields

$$m_r[\ddot{\theta} + \ddot{\alpha}(0)] + P\alpha'(0) + c_r\dot{\alpha}(0) + k_r\alpha(0) = 0 \tag{12}$$

Similarly, for the tip piece,

$$m_t[\ddot{\theta} + \ddot{\alpha}(l)] + P\alpha'(l) + c_t\dot{\alpha}(l) + k_t\alpha(l) = 0 \tag{13}$$

The above equations could be used to obtain the kernel $F(r,r_l)$ of Sec. II, but it is simpler (and illustrative) to proceed directly. Laplace transforms (with respect to time, with zero initial conditions) are taken of Eqs. (11-13). Equation (11) becomes an ordinary differential equation involving s, which is simply solved:

$$\tilde{\alpha}(s) = (A_\theta \sinh asy + B_\theta \cosh asy - 1)\tilde{\theta} \tag{14}$$

where A_θ, B_θ are obtained by solving Eqs. (12) and (13) simultaneously, which gives

$$\begin{bmatrix} A_\theta \\ B_\theta \end{bmatrix} = \frac{1}{\Delta}\begin{bmatrix} z_tC + asPS & -z_r \\ -(z_tS + asPC) & asP \end{bmatrix}\begin{bmatrix} c_rs + k_r \\ c_ts + k_t \end{bmatrix} \tag{15}$$

where

$$S \equiv \sinh als \qquad C \equiv \cosh als \qquad a^2 = \sigma w/P$$

and

$$z_{r,t} \equiv (ms^2 + cs + k)_{r,t}$$

$$\Delta(s) = asPCz_t + a^2s^2P^2S - (z_rz_tS + asPCz_r) \tag{16}$$

The relation between T and θ can be easily derived, since

$$T = \frac{1}{12} w^2 [m_r\ddot{\alpha}(0) + m_t\ddot{\alpha}(l) + (m_r + m_t)\ddot{\theta}]$$

$$+ \sigma w\int_0^l \int_{-w/2}^{w/2} x^2\ddot{\alpha}(y)\,dx\,dy \tag{17}$$

Taking the Laplace transform and making the appropriate substitutions,

$$\tilde{T}(s) = I_{ae}(s)s^2\tilde{\theta} \tag{18}$$

where I_{ae} is the inertance:

$$I_{ae} = \frac{1}{12}\sigma w^3 l\left[\left(\frac{C-1}{asl} + m_t^*S\right)A_\theta + \left(\frac{S}{asl} + m_r^* + m_t^*C\right)B_\theta\right]$$

$$m_t^* \equiv m_t/\sigma wl \qquad m_r^* \equiv m_r/\sigma wl \tag{19}$$

This result, obtained with remarkable ease compared to the modal expansion approach, includes damping: I_{ae} depends on (c_r,c_t) as well as (k_r,k_t) through Eq. (15). The inertance is analogous to inertia for a rigid body; indeed it can be shown that

$$\lim_{s\to 0} I_{ae}(s) = I_a \equiv \text{rigid inertia} \tag{20}$$

There are two symmetrically located arrays on Hermes. This permits uncoupling of translation and rotation of the rigid body. In symmetric twisting of the two arrays, the rigid-body motion in response to external torques can be seen to obey

$$T_e(s) = I_e(s)s^2\theta \qquad I_e(s) = I_b + 2I_{ae}(s) \tag{21}$$

Once again, $I_e(0)$ is the rigid moment of inertia (I_b = rigid body inertia). This shows the ease of combining inertance expressions of constituent bodies of a spacecraft. This can be done regardless of the methods used to obtain $I_{ae}(s)$, including approximate ones.

IV. Comparison with Modal Results

The closed-form results of Eqs. (19) and (21) are not directly comparable to modal results in the literature, for the latter exclude damping. Several special cases can be compared, however. Without damping, one obtains the result[4]:

$$I_e(s) = I\left(1 + \sum_{n=1}^{\infty}\frac{s^2k_n}{s^2+\omega_n^2}\right)^{-1} \tag{22a}$$

$$= I\left(1 - \sum_{n=1}^{\infty}\frac{s^2K_n}{s^2+\Omega_n^2}\right) \tag{22b}$$

where I = rigid inertia.

The (ω_n,Ω_n) are termed the unconstrained and constrained natural frequencies respectively.[4] The $\{\omega_n\}$ are the zeroes of $I_e(s)$, i.e., natural frequencies of the entire spacecraft (since at ω_n, external torque = 0). The $\{\Omega_n\}$ are poles of $I_e(s)$—from Eq. (21), also the poles of $I_{ae}(s)$, i.e., natural frequencies of the appendages alone (since from Eq. (18), $\theta = 0$, and the support point is motionless). In the case treated in Ref. 4, $k_t = c_t = c_r = 0$, $k_r \to \infty$, and the root mass m_r is included in the rigid-body inertia, hence $m_r = 0$. For this simplest case, Eq. (19) is reduced to

$$I_{ae}(s) = \frac{\sigma w^3}{12as}\frac{aPS + m_tsC}{aPC + m_tsS} \tag{23}$$

Clearly, both poles and zeroes of Eq. (23) lie on the imaginary axis. Putting $s = j\omega$, and setting the denominator to zero, gives the same equation as derived in Ref. 4 for the constrained frequencies. Setting the numerator of $I_e(j\omega)$ corresponding to Eq. (23) to zero gives the equation in Ref. 5 for unconstrained frequencies. Finally, since Eq. (23) has an infinite number of distinct poles, a partial-fraction expansion of it can be carried out, once the $\{\Omega_n\}$ are known. Then one obtains Eq. (22b), the $\{K_n\}$ being found as coefficients in the partial-fraction expansion. This result for K_n agrees with the (closed form) result in Ref. 4, derived by modal techniques. Details of all these equivalences are available in Ref. 5.

V. Truncation Errors

Truncation of the infinite sums in Eq. (22) is unavoidable for time-domain simulation. The closed-form expansion Eq. (23), and the corresponding $I_e(s)$, are directly useful in frequency-domain methods for control system analysis and design. Comparing Eq. (23) with truncated versions of Eq. (22) is of obvious interest. Attitude response is obtained from

$$\theta(s) = s^{-2}I_e^{-1}(s)\,T_e(s) \tag{24}$$

From Eq. (22a) it appears that

$$I_{eu}^{-1}(N;s) \triangleq \frac{1}{I}\left(1+\sum_{n=1}^{N}\frac{s^2 k_n}{s^2+\omega_n^2}\right) \tag{25}$$

is the correct expression for the exact I_e^{-1} to N terms in its partial-fraction expansion. The only errors arise from truncation, for a given $T_e(s)$. However, even the truncated inverse of Eq. (22b) is incorrect, for

$$I_{ec}^{-1}(N;s) \triangleq \frac{1}{I}\left(1-\sum_{n=1}^{N}\frac{s^2 K_n}{s^2+\Omega_n^2}\right)^{-1} = \frac{1}{I}\left(1+\sum_{n=1}^{N}\frac{s^2 k_n'}{s^2+\omega_n'^2}\right) \tag{26}$$

This incurs additional errors due to the approximations $k_n' \approx k_n$, $\omega_n \approx \omega_n$. This indicates that for given N, the U (unconstrained)-mode expansion gives better simulation accuracy. When expanding I_e rather than I_e^{-1}, the same reasoning indicates C (constrained) modes to be better.

A quantitative comparison of I_e with $I_{eu}(N)$ and $I_{ec}(N)$ is best carried out in dimensionless terms. The nondimensionalization scheme will reduce the number of significant spacecraft parameters. Hence, we introduce the parameters

$$m_t^* \equiv m_t/\sigma w l^2 \qquad I_b^* \equiv I_b/I \qquad I_e^*(s) \equiv I_e(s)/I$$

and

$$\omega^* \equiv \omega/\Omega$$

where

$$\Omega = (\sigma w l^2/P)^{1/2} \tag{27}$$

Here Ω^* is a flexibility parameter, and m^*, I_b^* are mass parameters. The effect of decreasing Ω is to reduce the spacing between dimensional frequencies, and I_b^* corresponds to the degree to which the spacecraft is rigid. As $I_b^* \to 1$, the frequencies $\{\Omega_n\}$, $\{\omega_n\}$ coalesce[4] since the spacecraft becomes almost rigid.

We are now ready for quantitative comparisons. Of particular interest are the errors

$$\begin{aligned} \Delta I_{ec} &\equiv I_{ec}(N) - I_e & \Delta I_{eu} &= I_{eu}(N) - I_e \\ \Delta I_{ec}^{-1} &\equiv I_{ec}^{-1}(N) - I_e^{-1} & \Delta I_{eu}^{-1} &= I_{eu}^{-1}(N) - I_e^{-1} \end{aligned} \tag{28}$$

where a dependence on s is understood. It follows directly that

$$\Delta I_{ec} = \sum_{n=N+1}^{\infty}\frac{s^2 K_n}{s^2+\Omega_n^2} \qquad \Delta I_{eu}^{-1} = -\sum_{n=N+1}^{\infty}\frac{s^2 k_n}{s^2+\omega_n^2} \tag{29}$$

in appropriate nondimensional terms. Clearly, ΔI_{ec} becomes unbounded at frequencies $\{\Omega_n, n>N\}$, and ΔI_{eu}^{-1} becomes unbounded at $\{\omega_n, n>N\}$. In practice, this difficulty is obviated by the fact that the torques $T_e(s)$ usually have finite bandwidth. Therefore, comparisons are made only for frequencies below ω_{n+1} or Ω_{N+1}, as the case may be.

Consider first a relatively flexible spacecraft, with $m^* = 0.5$, $I_b^* = 0.1$, and $\Omega^* = 1.0$. Figure 5 shows the errors incurred with just one mode: $N=1$. The dashed lines mark the exact C-frequencies or poles of I_e, and the dotted lines mark exact U-frequencies or zeroes of I_e. Even with $N=1$, it is clear that for a given accuracy (of simulation results), the unconstrained expansion is valid over a larger range of ω^*. However, for an applied torque of bandwidth $< \approx 1.7$, the C-expansion gives more accurate results. These observations are in accord with the author's simulation experience. Note, however, that the inertance itself is better approximated by C-modes.

Taking a larger N does not change these conclusions. The case $N=4$ is shown in Fig. 6, over a larger range of ω^*. Only errors in I_e^{-1} (corresponding to simulation accuracy) are shown. The error ΔI_{ec}^{-1} becomes unbounded at the exact U-frequencies, i.e., poles of I_e^{-1}. This is borne out by Eq. (26), which shows that at $s = j\omega_n$, while $I_e \to \infty$, I_{ec}^{-1} remains finite.

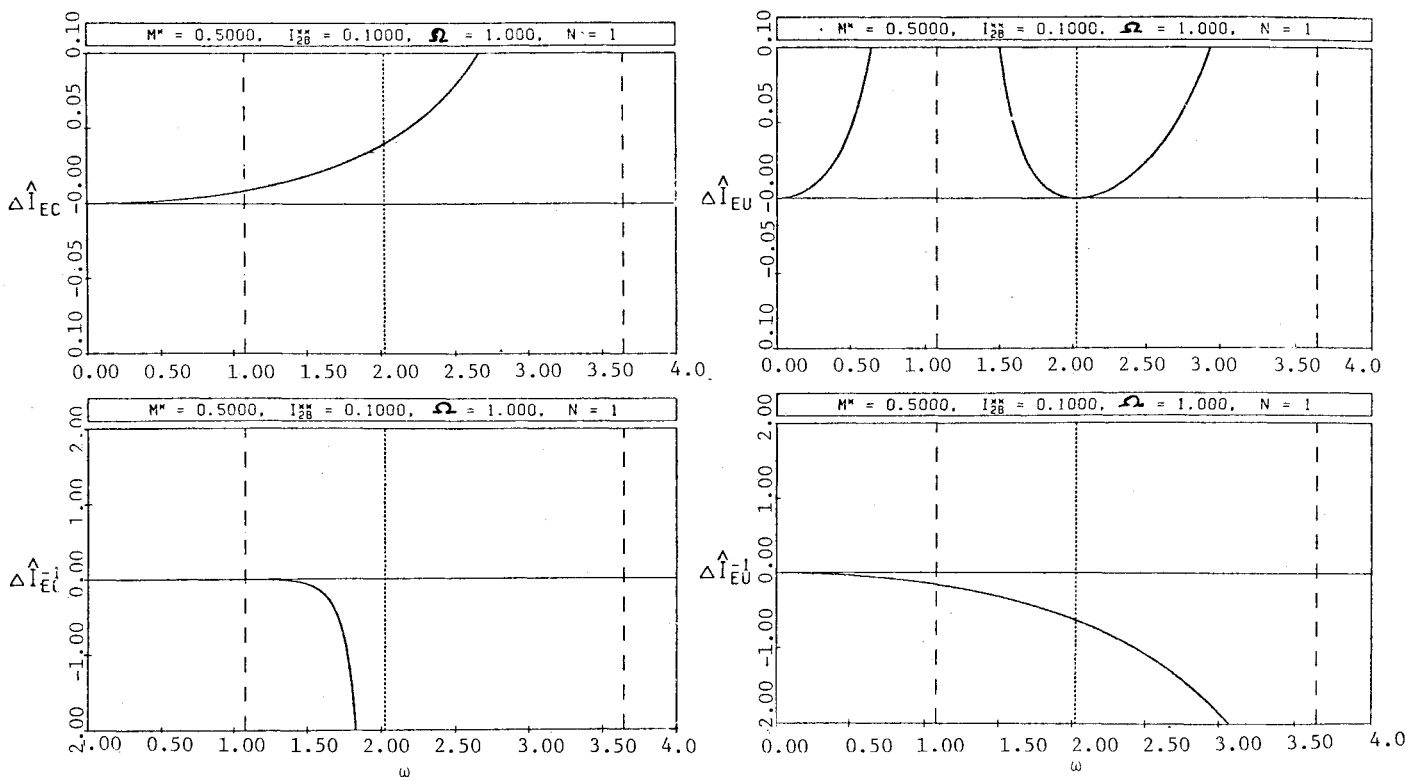

Fig. 5 Errors in inertance and inverse inertance for one mode.

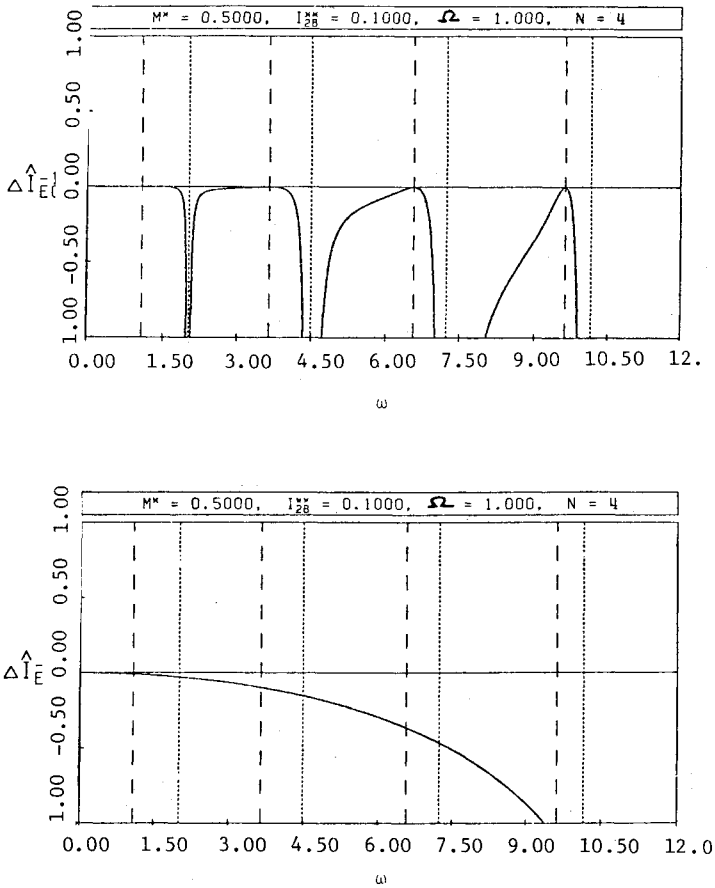

Fig. 6 Inverse inertance errors—model parameters as shown, $N=1$.

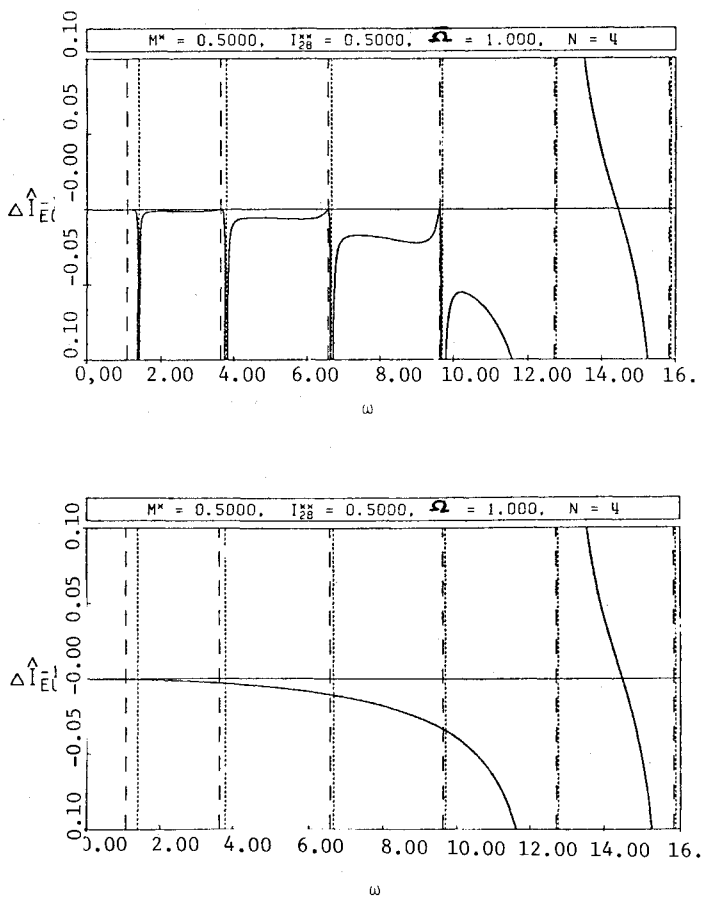

Fig. 7 Inverse inertance errors—model parameters as shown, $N=4$.

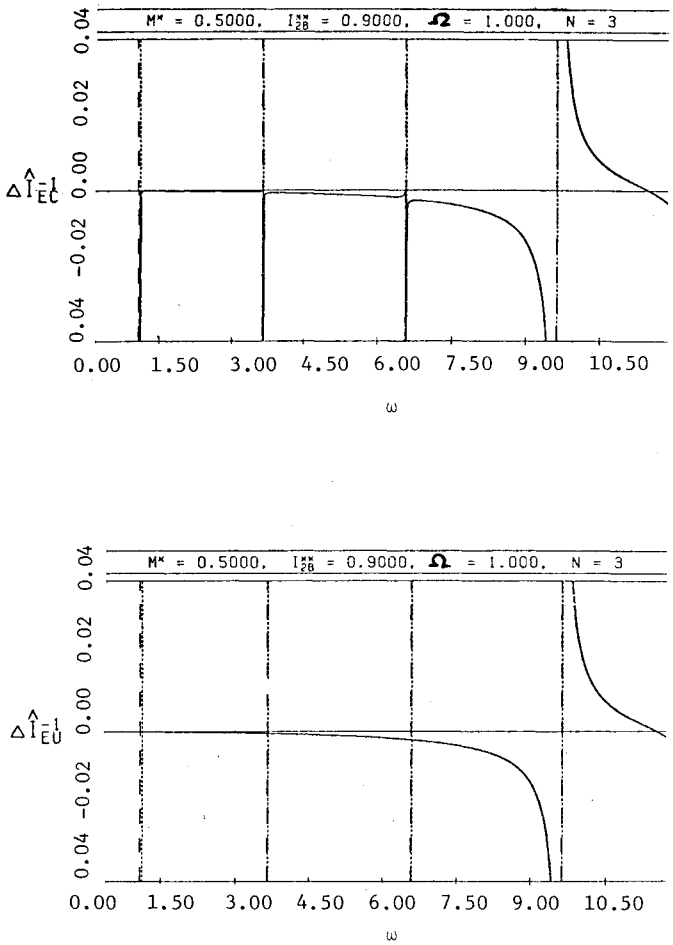

Fig. 8 Inverse inertance errors for "more rigid" case—model parameters as shown.

It also shows that at $s=j\Omega_n$, both I_{ec}^{-1} and I_e^{-1} are zero, which explains the zero error at $\{\Omega_n\}$ in Fig. 6 (Ω_n indicated by dashed lines). I_{ec}^{-1} is zero for all Ω_n, even for $n>N$.

Consider now a "more rigid" spacecraft, with $I_b^*=0.5$, and $m^*=0.1$, $\Omega^*=1$ as before. The errors in I_e^{-1} with $N=4$ are shown in Fig. 7. With increased I_b^*, the separation between Ω_n and ω_n (for equal n) is reduced. This means that the C-expansion is valid over a larger portion of the ω axis. It is, however, still preferable to use the U-modes for simulation. An even more rigid case, with $I_b^*=0.9$ and $N=3$, is shown in Fig. 8. In this case, the dashed (Ω_n) and dotted (ω_n) lines are practically coincident. Of course, this coincidence is not exact, and I_{ec}^{-1} ($j\omega_n$) is still unbounded. However, except at these singularities, the errors ΔI_{ec}^{-1} and ΔI_{eu}^{-1} are remarkably similar. Thus I_{ec}^{-1} and I_{eu}^{-1} may appear to be equally appropriate for simulation, but gross errors will still result if the torque spectrum contains energy near $s=j\omega_n$.

The effect of damping will no doubt be to eliminate singularities along the imaginary axis. It is only necessary to expand Eq. (21), with c_r, $c_t\neq 0$, in partial fractions yielding

$$I_e^{-1}(s)=\frac{1}{I}\left[1+\sum_{n=1}^{\infty}\frac{s^2k_n}{s^2+2\zeta_n\omega_n s+\omega_n^2}\right] \tag{30}$$

The damping factors ζ_n are simply calculated. The power of this frequency-domain approach is seen by comparing the ease of obtaining Eq. (30) with a similar analysis for the damped case, which would require using complex modes and orthogonality conditions.

VI. Mean-Square Errors

Another approach to obaining truncation errors is based on Parseval's theorem for a given signal x:

$$\int_0^\infty x^2(t)\,dt = \frac{1}{2\pi}\int_{-\infty}^{\infty} |\tilde{x}(j\omega)|^2 d\omega \tag{31}$$

Now let x be the simulation error in the response $\tilde{\theta}$ to a torque $\tilde{T}_e(s)$:

$$\tilde{x}(s) = (1/s^2)\Delta I_{eu}^{-1}(N;s)\,T_e(s) \tag{32}$$

where ΔI_{eu}^{-1} is given by Eq. (29). Now, Eq. (31) yields the integrated mean-square simulation error in the impulse response ($\tilde{T}_e = 1$), denoted ϵ_N, given by

$$\epsilon_N = \frac{1}{2\pi}\int_{-\infty}^{\infty} \frac{1}{\omega^2} |\Delta I_{eu}^{-1}(N;j\omega)|^2 d\omega \tag{33}$$

where ΔI_{eu}^{-1} for N terms is given by the second of Eqs. (29). However, upon substituting Eq. (29) into Eq. (33) and integrating, one obtains an infinite value for ϵ_N. Physically, this occurs because the error $x(t)$ consists of terms of the form $b_n \sin\omega_n t$, which are not square-integrable functions. In practice, the torque $T_e(s)$ is band-limited, reducing the error. However, if $T_e(s)$ contains finite energy at any spacecraft frequency ω_n, then, in the undamped case, infinite mean-square error will result.

A meaningful result can be obtained when the damped case, Eq. (30), is considered. If only N modes are kept, we obtain

$$\epsilon_N = \frac{1}{\pi}\int_0^\infty \frac{1}{\omega^2}\left|\sum_{N+1}^{\infty} \frac{\omega^2 k_n}{\omega_n^2 - \omega^2 + 2j\zeta_n\omega_n\omega}\right|^2 d\omega \tag{34}$$

It is difficult to evaluate this integral directly; however, upper and lower bounds on its value can be obtained from the inequalities

$$\int |x|^2 du \geq \left|\int x\,du\right|^2 \qquad \left|\sum_n x_n\right|^2 \leq \sum_n |x_n|^2$$

The first inequality, evaluating the integral by partial fractions, gives only that $\epsilon_N > 0$. The second inequality can be evaluated similarly, yielding

$$\epsilon_N \leq \sum_{n=N+1}^{\infty} \frac{k_n}{8\omega_n^3 \sin\theta_n} \tag{35}$$

where

$$\theta_n = \tfrac{1}{2}\sin^{-1} 2\zeta_n\sqrt{1-\zeta_n^2}$$

Since usually, only small damping will be provided, $\zeta_n \ll 1$, particularly for large n. Hence Eq. (35) simplifies to

$$\epsilon_N < \sum_{n=N+1}^{\infty} \frac{k_n}{8\zeta_n\omega_n^3} \tag{36}$$

This result confirms that the upper bound $\to\infty$ as $\zeta_n \to 0$. In its present form, it is not directly useful. However, it may be possible to derive an identity for the sum Eq. (36) from $n=1$ to ∞. Similar modal identities have been derived for the undamped case.[4] However, as of this writing, an identity for the damped case, applicable to Eq. (30), remains in the future.

VII. Concluding Remarks

The main contribution of the present paper has been to show that frequency-domain dynamics analysis can be economical and productive. Especially for multicomponent structures, including discrete springs and dampers, this approach is convenient. In principle, the analysis could be extended to linearly elastic structures composed of all-flexible bodies. Each type of component structure—e.g., a Hermes-type solar array—can be analyzed in advance, once and for all, and used in deriving the analogs of Eqs. (7) and (8).

The analysis of truncation errors given in Sec. IV, establishes conclusively that (at least for this problem) for simulation purposes, U-modes or spacecraft modes give more accurate results than C- or appendage modes. The only exception to this occurs if the input torque bandwidth is of the order of Ω_1, as seen from ΔI_{ec}^{-1} in Fig. 5. Some general features of the quantitative results in Figs. 5-8, such as singularities and zeroes of $\Delta I_{eu}^{-1}(s)$ and $\Delta I_{ec}^{-1}(s)$, clearly apply in the general context of Sec. I. The relative advantage of using U-modes increases with increasing flexibility. This would indicate that for all-flexible structures, natural modes of constituent bodies would be highly inappropriate for simulation purposes.

Several applications of this approach are possible in combination with frequency domain control theory. Nyquist stability analysis, root locus plots, analysis of feedback control systems, are all feasible, and are quite accurate and convenient when the exact $I_e^*(s)$ is available. There have been rapid advances lately in multivariable controller design using transfer matrices, and for nonlinear systems, e.g. using positivity theorems.[6] The telescoping of a large or infinite-order state space into finite-order transfer matrices leads to obvious savings. Most flexible spacecraft yield completely controllable and observable systems, so that this economy is useful. In many spacecraft, such as the example chosen, single-input single-output systems (with infinite-order state space) result with clear advantages in controller design. The author hopes to see increased application of frequency-domain methods in both dynamics and control.

Acknowledgments

This research was supported by the National Research Council of Canada under Grant No. S7309, and was conducted entirely while the author was a research associate at the University of Toronto. Computational assistance was ably rendered by Mr. G. D'Eleuterio.

References

[1] Poelaert, D.H.L., "Dynamic Analysis of Non-Rigid Spacecraft," *Proceedings of the Symposium on Large Flexible Spacecraft*, Blacksburg, Va., June 1977.

[2] MacFarlane, A.G.J., "The Development of Frequency-Response Methods in Automatic Control," *IEEE Transactions on Automatic Control*, Vol. AC-24, No. 2, April 1979.

[3] Hughes, P.C., "Dynamics of Flexible Space Vehicles with Active Attitude Control," *Celestial Mechanics*, Vol. 9, 1974, pp. 21-39.

[4] Hughes, P.C. and Garg, S.C., "Dynamics of Large Flexible Solar Arrays and Application to Spacecraft Attitude Control System Design," University of Toronto, Institute for Aerospace Studies, Rept. 179, Feb. 1973.

[5] Garg, S.C., "Active Control of Dynamics Transfer Functions for a Flexible Spacecraft," University of Toronto, Institute for Aerospace Studies, Rept. 239, Sept. 1980.

[6] Iwens, R.P., Benhabib, R.J., and Jackson, R.L., "A Unified Approach to the Design of Large Space Structure Control Systems," *Proceedings JACC*, Paper No. FP1-A, Aug. 1980.